2009 IEEE/ASME International Conference on Advanced Intelligent Mechatronics
Suntec Convention and Exhibition Center
Singapore, July 14-17, 2009

Organized Sensor Network Design for Active Feedback Control

Shaohui Foong, *Student Member*, *IEEE/ASME*, and Kok-Meng Lee, *Fellow*, *IEEE/ASME*

***Abstract*—Active continuous control of systems using physical sensors are hindered by presence of corrupting noise in discretized measurements which degrades performance. This paper presents a systematic development of organized sensor networks that fuses the dynamic implementation of parallel and sequential network architectures with conventional multi-sensor filtering techniques to improve performance through collaborative network enhancement of noise suppression and sampling rate. The classical control of an inverted pendulum using vision sensors is presented as an illustrative example. Simulation results suggest that an organized sensor network with dynamic throttling outperforms a static network while minimizing overall sensor utilization.**

I. Introduction

Rapid advances in low-cost computing technologies and low-power wireless communications within the last ten years have spawned a flurry of research and development on sensor networks which allows random deployment in inaccessible terrains or disaster relief operations. Commercial, military and potential sensor network applications (that include home, healthcare, military ISR, environment protection, water management, and livestock and endanger monitoring) can be found in a number of survey papers [1][2][3][4]. These developments, along with the availability of real-time machine vision systems at low cost, have provided the motivation to develop methods to remotely position mobile mechatronic devices (for applications such as structural health monitoring of large structures or compliant handling of natural or live objects for food processing).

In real time applications, physical sensors are used to observe and measure the system states for subsequent feedback control. A common issue encountered in remote control of mobile mechatronic devices is the tradeoff between responsiveness and the operating range of the sensor that often limits the accuracy of the controlled system. In the case of vision-based control, for example, images with higher resolutions are required in order to achieve more precise control, thereby increasing the computation overheads with additional pixels to be processed. In addition, vision sensors often exhibit measurement errors which could further degrade the controlled system performance. An effective alternative to overcome the above problems is to employ an organized sensor network with multi-sensor fusion.

Measurement errors of physical sensors can be classified as systematic and random errors. Unlike the former, random errors are stochastic in nature and although they cannot be predicted, they can be adequately modeled using stochastic models. Since these measurements occur in discrete intervals, the Discrete Kalman Filter (DKF) has been extensively and effectively used to estimate the true measurement from raw observations and prior knowledge of system dynamics [5][6][7].

To address the inherent latency and improve performance in vision based control, different sensor network architectures were investigated in [8]. In these studies, it was found that by sequentially activating vision sensors in a network, the maximum velocity that can be tracked was increased. Direct comparison between sequential and parallel architectures of sensor networks has been investigated in recent decades [6][7], and marginally favors sequential processing. However, there is a lack of a unified approach to amalgamate these two architectures in a complementary fashion. A network of sensors having elements of both architectures can improve the sensing performance two fold through reduction in overall sampling time and suppression of measurement noise.

Inspired by developments in dynamic sensor networks, where an energy efficient sensor network is achieved through adaptively adjusting network density and coverage quality [9], the performance of the sensor network can be adjusted and regulated just like a normal feedback controller. Such active management of the network reduces overall utilization of the entire sensor network while retaining the potential and capabilities of a fully operational sensor network.

As control of the classical inverted pendulum system has been successfully achieved through low-cost USB cameras [10][11], this will serve as a platform to facilitate the investigation and development of an organized sensor network that harnesses the elements of parallel and sequential architectures with the flexibility of dynamic networks in a systematic manner.

The remainder of this paper is arranged as follows:

- We systematically characterize and develop an organized sensor network that is fundamentally based on the temporal measurement model for a sensor. This temporal model allows the subsequent derivation of optimal weighting scheme between concurrent sensor measurements. The throttling controller which actively manages the network configuration is introduced as well.
- To compare and evaluate control performance of various sensor configurations and effectiveness of network

Manuscript received January 31, 2009. This work was supported in part by the Georgia Agricultural Technology Research Program and the U.S. Poultry and Eggs Association.

S. Foong and K.-M. Lee are with the Woodruff School of Mechanical Engineering at the Georgia Institute of Technology, Atlanta, GA 30332-0405 USA (e-mail: shao@gatech.edu; kokmeng.lee@me.gatech.edu).

Authorized licensed use limited to: IEEE Editors in Chief. Downloaded on February 5, 2010 at 14:16 from IEEE Xplore. Restrictions apply.

throttling, simulations of DKF assisted state feedback control of an inverted pendulum system in perfect (no noise) and practical (with noise) environments are used.

II. Organized Sensor Networks

Sensors in a network can be organized into s groups with each group containing r sensors that competitively and/or complementary sample some or all states of an n-order system. Graphically, the sensing states of the j^{th} sensor in the i^{th} group of the [s, r] network can be represented as shown in Fig. 1. As each network sensor has individual characteristics, an organized sensor network is implemented for active management.

Fig. 2 illustrates a control system using a network with [s, r] sequential and redundant sensors. It consists of a throttling controller, a weighting optimizer and a Kalman filter (DKF) working in tandem to produce a filtered estimate of the system states from noise corrupted individual sensor measurements. The throttling controller uses the desired controller output, sensor measurements and user defined performance specifications to determine the required [s, r] sensor configuration, and the optimal weighting distribution for each sensor group. Finally, the Kalman filter will utilize the weighted sensor measurements and system dynamics to generate a filtered estimate of the system states for subsequent control.

A measurement model that characterizes the system state measurement by each sensor in the [s, r] network is developed in the temporal domain.

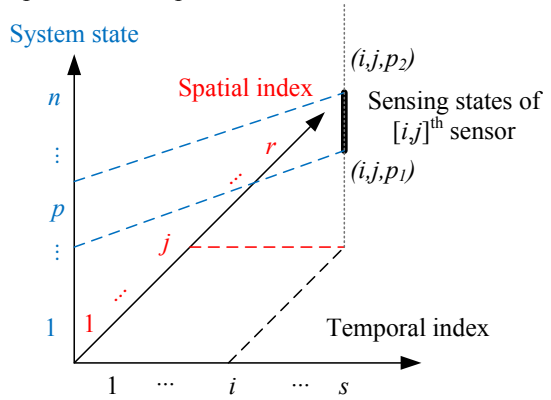

Fig. 1. Graphical representation of network organization.

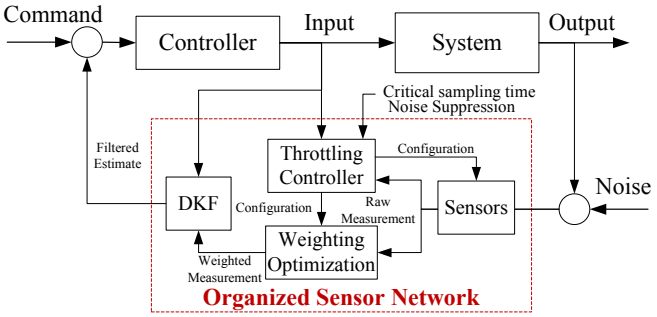

Fig. 2. Block diagram of an organized sensor network.

A. Sensor Temporal Measurement Model

The measurement of the state vector $\mathbf{x} \in \mathbb{R}^n$ by the j^{th} sensor of the i^{th} group in the sensor network at time t (with sampling period T_{ij}) is given by

$$\begin{cases} \mathbf{z}_{ij}(t) = \mathbf{L}_{ij}\left(\mathbf{x}(kT_{ij}) + \mathbf{v}_{ij}(kT_{ij}) + \mathbf{b}_{ij}\right) & \text{(1a)} \\ \mathbf{v}_{ij}(kT_{ij}) = [\sigma_{ij1}\cdots\sigma_{ijp}\cdots\sigma_{ijn}]^T \sim \mathrm{N}\left(0, \mathbf{\Psi}_{ij}(kT_{ij})\right) & \text{(1b)} \end{cases}$$

where $kT_{ij} \le t < (k+1)T_{ij}$; k is the time index integer, $\mathbf{b}_{ij}$ and $\mathbf{v}_{ij} \in \mathbb{R}^n$ are the bias and uncorrelated zero-mean Gaussian white measurement noise with covariance $\mathbf{\Psi}_{ij} \in \mathbb{R}^{n\times n}$; and the measurement matrix is

$$\mathbf{L}_{ij}\left(\in \mathbb{R}^{n\times n}\right) = \mathrm{diag}(\delta_{ij1}\cdots\delta_{ijp}\cdots\delta_{ijn}) \quad (2)$$

where $\delta_{ijp} = \begin{cases} 1 & \text{if } x_p \text{ is measurable} \\ 0 & \text{otherwise} \end{cases}$

If all states are measurable, $\mathbf{L}_{ij}$ is an identity matrix. Similarly, if x_p is measurable,

$$\mathbf{\Psi}_{ij}\left(kT_{ij}\right) = \mathrm{diag}\left(\psi_{ij1}(kT_{ij})\cdots\psi_{ijp}(kT_{ij})\cdots\psi_{ijn}(kT_{ij})\right) \quad (3)$$

where ψ_{ijp} is the variance associated with σ_{ijp}.

B. Weighting coefficients Optimization

The effective noise variance is minimized through constrained optimization. Without the loss of generality, we restrict our model to an [s, r] network with homogeneous sampling time T_{ij}=T_c as an illustration. In this network, the simultaneous sampling of r sensors by the i^{th} group provides a sequential weighed measurement $\bar{\mathbf{z}}_i$ at time t where $\left(kT + T_i\right) \le t < (k+1)T + T_i$:

$$\begin{cases} \bar{\mathbf{z}}_i(t) = \bar{\mathbf{L}}_i\left(\mathbf{x}(kT+T_i) + \bar{\mathbf{v}}_i(kT+T_i) + \bar{\mathbf{b}}_i\right) & \text{(4a)} \\ \bar{\mathbf{v}}_i(kT+T_i) = \sum_{j=1}^{r} \boldsymbol{\alpha}_{ij}\mathbf{v}_{ij}(kT+T_i) \sim \mathrm{N}(0, \bar{\mathbf{\Psi}}_i(kT+T_i)) & \text{(4b)} \end{cases}$$

and $$T_i = (i-1)(T_c / s). \quad (4c)$$

In 4(a) and 4(b), the over-bar "–" indicates that the quantity is weighted in the i^{th} sensor group. In (4a),

$$\bar{\mathbf{L}}_i = \mathrm{diag}(\bar{\delta}_{i1}\cdots\bar{\delta}_{ip}\cdots\bar{\delta}_{in}) \quad (5)$$

where $\bar{\delta}_{ip} = \max(\delta_{i1p}\cdots\delta_{ijp}\cdots\delta_{irp})$. Similarly, the weighted bias and noise covariance matrix are given by (6) and (7):

$$\bar{\mathbf{b}}_i = \sum_{j=1}^{r} \boldsymbol{\alpha}_{ij}\mathbf{b}_{ij} \quad \text{where } \boldsymbol{\alpha}_{ij} \in \mathbb{R}^{n\times n} \quad (6)$$

$$\boldsymbol{\alpha}_{ij} = \mathrm{diag}(a_{ij1}\cdots a_{ijp}\cdots a_{ijn}) \text{ and } \sum_{j=1}^{r} \boldsymbol{\alpha}_{ij} = \mathbf{I}_n \quad (6a,b)$$

$$\bar{\mathbf{\Psi}}_i = \mathrm{diag}(\bar{\psi}_{i1}\cdots\bar{\psi}_{ip}\cdots\bar{\psi}_{in}) \text{ where } \bar{\psi}_{ip} = \sum_{j=1}^{r} a_{ijp}^2\psi_{ijp} \quad (7a,b)$$

Hence, each sensor group contains r weighting coefficients to be selected for each of the n system states. One method to uniquely resolve for the $r\times n$ coefficients is by determining the coefficients that minimizes $\bar{\mathbf{\Psi}}$. For this, the first $(r-1)$ noise variance in (7b) is expressed as a multiple of the r^{th} variance, which yield

$$\bar{\psi}_{ip} = \left(a_{i1p}^2 m_{i1p} + \cdots + a_{i(r-1)p}^2 m_{i(r-1)p} + a_{irp}^2\right)\psi_{irp} \quad (8)$$

Authorized licensed use limited to: IEEE Editors in Chief. Downloaded on February 5, 2010 at 14:16 from IEEE Xplore. Restrictions apply.

where m_{ijp} is a known positive gain. Taking partial derivatives of (8) with respect to a_{ijp} (for j=1…r–1) and equating them to zero, (r–1) equations can then be obtained for computing the optimal weighting coefficients a_{ijp}:

$$\frac{\partial \bar{\psi}_{jp}}{\partial a_{ijp}} = m_{ijp} a_{ijp} + \sum_{j=1}^{r-1} a_{ijp} - 1 = 0 \qquad (9)$$

Example:

Table 1 shows the computed optimal weighting coefficients where the subscripts (i, p) are omitted for readability for a network with 1, 2, 3 and 4 sensor redundancy.

Table 1. $(a_1 \ \cdots \ a_r)$ for the [s, r] network configuration.

[s, 1]	$a_1 = 1$
[s, 2]	$(a_1 \quad a_2) = \dfrac{(1 \quad m_1)}{m_1 + 1}$
[s, 3]	$(a_1 \quad a_2 \quad a_3) = \dfrac{(m_2 \quad m_1 \quad m_1 m_2)}{m_1 + m_2 + m_1 m_2}$
[s, 4]	$(a_1 \quad a_2 \quad a_3 \quad a_4) = \dfrac{(m_2 m_3 \quad m_1 m_3 \quad m_1 m_2 \quad m_1 m_2 m_3)}{m_1 m_2 + m_1 m_3 + m_2 m_3 + m_1 m_2 m_3}$

The normalized weighted variance for [s ,2] and [s ,3], which are computed using (7b) with unit covariance of the r^{th} variance and the coefficients in Table 1, are plotted as a function of the gains m_1 and m_2 in Fig. 3(a) and 3(b). From both plots, the curve and surface approach unity asymptotically as m_1 and m_2 increase. Hence the inclusion of measurement from an additional sensor (no matter how noisy) will reduce the effective variance. It is noted that this weighting optimization is not restricted to the classical Gaussian noise distribution discussed here.

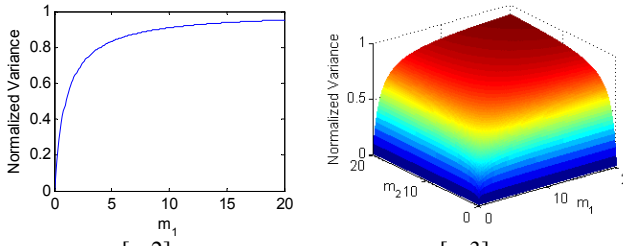

[s, 2] [s, 3]

Fig. 3. Normalized effective variance for [s, 2] and [s, 3].

C. Discrete Kalman Filtering

As an illustration, we consider here a plant in continuous-time state-space representation with a controllable input **u**:

$$\begin{cases} \dot{\mathbf{x}}(t) = \mathbf{A}\mathbf{x}(t) + \mathbf{B}\mathbf{u}(t) \\ \mathbf{y}(t) = \mathbf{C}\mathbf{x}(t) + \mathbf{D}\mathbf{u}(t) \end{cases} \qquad (10)$$

The corresponding discrete-time representation with process noise **ω** of covariance **Ω** is given by

$$\begin{cases} \mathbf{x}((k+1)T) = \mathbf{F}\mathbf{x}(kT) + \mathbf{G}\mathbf{u}(kT) + \boldsymbol{\omega}(kT) \\ \mathbf{y}(kT) = \mathbf{C}\mathbf{x}(kT) + \mathbf{D}\mathbf{u}(kT) \end{cases} \qquad (11)$$

where $\mathbf{F}(T) = e^{\mathbf{A}T}$; $\mathbf{G}(T) = \int_0^T e^{\mathbf{A}\lambda} d\lambda \, \mathbf{B}$ and T=T_c/s. Without the loss of generality, the control law of the linear system using full state feedback (FSF) is

$$\mathbf{u}(kT \le t < (k+1)T) = -\mathbf{K}_F \hat{\mathbf{x}}(kT) \qquad (12)$$

where $\mathbf{K}_F$ is the feedback matrix; and $\hat{\mathbf{x}}(kT)$ is the estimate of $\boldsymbol{x}$ at t=kT. The discrete Kalman filter [12] adapted for an [s, r] sensor-networked FSF system can be summarized by

$$\mathbf{K}(kT) = \mathbf{P}(kT)\left[\mathbf{I} + \bar{\boldsymbol{\Psi}}^{-1}(kT)\mathbf{P}(kT)\right]^{-1} \bar{\boldsymbol{\Psi}}^{-1}(kT) \qquad (13)$$

$$\hat{\mathbf{x}}((k+1)T) = \mathbf{F}\hat{\mathbf{x}}(kT) - \mathbf{G}\mathbf{K}_F\hat{\mathbf{x}}(kT) + \mathbf{F}\mathbf{K}(kT)\left(\bar{\mathbf{z}}(kT) - \hat{\mathbf{x}}(kT)\right) \qquad (14)$$

$$\mathbf{P}((k+1)T) = \mathbf{F}\mathbf{P}(kT)\left[\mathbf{I} + \bar{\boldsymbol{\Psi}}^{-1}(kT)\mathbf{P}(kT)\right]^{-1} \mathbf{F}^T + \boldsymbol{\Omega}(kT) \qquad (15)$$

where **K** and **P** are the gain and estimate error covariance of the Kalman filter.

D. Throttling Controller

In an [s, r] network, a controller is required to select the desired sensor configuration out of a myriad of possible sensor configurations. For example, a three-sensor network contains five possible sensor configurations as illustrated in Fig. 4, where each arrow in the acquisition timing diagram represents the measurement input from a solitary sensor.

A direct method that expresses the scalar integer quantities of r and s at a future time t=(k+1)T as functions of all observable and measurable variables and parameters at the current time t=kT can be expressed by:

$$r((k+1)T) = f\left(\hat{\mathbf{x}}(kT), c(kT), \mathbf{u}(kT)\right) \qquad (16a)$$

$$s((k+1)T) = g\left(\hat{\mathbf{x}}(kT), c(kT), \mathbf{u}(kT)\right) \qquad (16b)$$

where c is the desired command of the system.

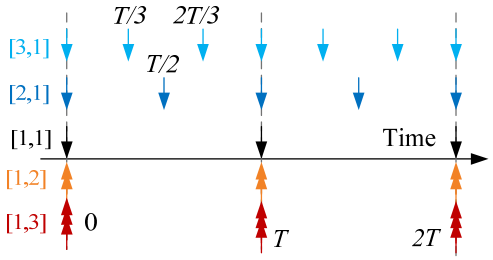

Fig. 4. Acquisition schedule of different sensor configurations.

III. Simulation Results And Discussions

We investigate the effects of utilizing sensor networks on the controlled system performance under the influences of process and measurement noise. For numerical validation and performance evaluation, the inherently unstable inverted pendulum system (Fig. 5 along with the parameter values in Table 2) where analytical solutions are available for validation, is chosen in this study. The system is under FSF control with optical cameras which has the advantage of measuring all state variables individually and simultaneously.

Table 2. Simulation parameters of inverted pendulum.

System Parameters	l_p=0.5m; m_p=0.2kg; m_c=0.5kg; g=9.81ms^{-2}
Process Noise	$\boldsymbol{\Omega}$ = diag(0.015,0.002,0.15,0.15)
FSF Gains	$\mathbf{K}_F$ = [-26.9 -97.0 -23.9 -24.7]
Sensor Parameters	T_c = 0.1s; $\mathbf{L}_{ij}$ = $\mathbf{I}$,, $\mathbf{b}_{ij}$ = 0
Measurement Noise	$\boldsymbol{\Psi}_{ij}$ = diag(0.15^2,0.1^2,0.1^2,0.1^2)
DKF IC	$\mathbf{P}(0) = \boldsymbol{\Sigma}$, $\hat{\mathbf{x}}(0) = 0$

Authorized licensed use limited to: IEEE Editors in Chief. Downloaded on February 5, 2010 at 14:16 from IEEE Xplore. Restrictions apply.

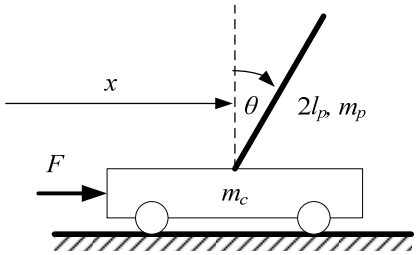

Fig. 5. Schematic of inverted pendulum.

The linearized equation of the pendulum motion is given by (17) where $\mathbf{x} = \begin{bmatrix} x & \theta & \dot{x} & \dot{\theta} \end{bmatrix}^{\mathrm{T}}$:

$$\dot{\mathbf{x}}(t) = \begin{bmatrix} \mathbf{0}_{22} & \mathbf{I}_{22} \\ \mathbf{A}_{21} & \mathbf{0}_{22} \end{bmatrix} \mathbf{x}(t) + \begin{bmatrix} \mathbf{B}_1 \\ \mathbf{B}_2 \end{bmatrix} \mathbf{u}(t) \tag{17}$$

where $\mathbf{A}_{21} = \frac{1}{Ml_p} \begin{bmatrix} 0 & -3m_p g l_p \\ 0 & 3(m_p + m_c)g \end{bmatrix}$; $\mathbf{B}_2 = \frac{1}{Ml_p} \begin{bmatrix} 4l_p \\ -3 \end{bmatrix}$;

$\mathbf{0}_{22}$ and $\mathbf{I}_{22}$ are the 2×2 null and identity matrixes respectively; $\mathbf{B}_1 = \begin{bmatrix} 0 & 0 \end{bmatrix}^{\mathrm{T}}$ and $M = \left(m_p + 4m_c \right)$.

The FSF gains are computed to place the desired closed-loop poles at –10, –8, –3 and –3. Modeled after an industrial network vision system [13], the optical camera, capable of sampling all four state variables at 10 frames per second (fps), has a sampling time $T_{ij}=T_c=0.1$s. To ensure asymptotic stability under FSF, the maximum sampling time of the discretized system is T_{crit} (or 0.0858 seconds for FSF gains in Table 2). The [s>1,r] ([1,r] would result in an unstable system) sensor network will possess an effective sampling rate of $T=T_c/s$.

Two performance criteria, command error (CE) and filtered measurement error (FE) are defined for the cart displacement over N measurements in (18a) and (18b):

$$\mathrm{CE} = \int_0^{NT} \left(c(t) - x(t) \right)^2 dt \; ; \tag{18a}$$

$$\mathrm{FE} = \sum_{k=0}^{N-1} \int_{kT}^{(k+1)T} \left(\hat{x}(kT) - x(t) \right)^2 dt \tag{18b}$$

where c is the desired cart command. Since, in presence of noise, the time responses (and consequently the FE and CE) vary from simulation to simulation, the convergence of the mean and standard deviation (SD) of FE and CE as a function of number of simulation runs are statistically studied. From Fig. 6, it can be seen that at least 200 runs are required for sufficient convergence of FE and CE.

A. Effects of Network Configurations

The following cases were simulated:

[s>1, 1]: in the noise-free environment and zero sensor bias: This is equivalent to investigating the effect of the different sampling period T_c/s on the system. The special case [∞, 1] is analogous to a continuous-time system (T→0 as s→∞) which serves as a basis for comparison. The transient and steady-state results (compared against [∞, 1]) are plotted in Fig. 7, where only the first 0.5 second of the unit step response is shown in Fig. **7**(a) to magnify the differences during transient.

[2,1]: The interest here is to investigate the effect of sensor network on the stable system (with zero mean *Gaussian* white process and measurement noise as specified in Table 2) by comparing with/without Filter for the same sampling period of $T=T_c$/s:

- No measurement noise: $\mathbf{u}(t) = -\mathbf{K}_F \mathbf{x}(kT)$
- No filter: $\mathbf{u}(t) = -\mathbf{K}_F \bar{\mathbf{z}}(kT)$
- With DKF: $\mathbf{u}(t) = -\mathbf{K}_F \hat{\mathbf{x}}(kT)$

Table 3 compares the effects of using the DKF on CE and FE. Snapshot comparisons of the time responses are given in Fig. 8(a).

[*s*, *r*]: To provide insights into trade-offs between sensor redundancy and effective sampling time for a total number of sensors, additional sensor network configurations are compared statistically. Fig. 8(b) and (c) shows the effect on the time responses of the cart due to alterations in r and s independently. With [2,2] as a basis for comparison, the data are tabulated in Table 4 along with a surface plot relating CE/FE to the number of sensors in redundancy and sequential configuration in Fig. 9.

For each case, 500 simulation runs were executed and in each independent simulation, the same Gaussian noise is applied to all cases (type of filtering in Table 3 and configuration in Table 4) being studied.

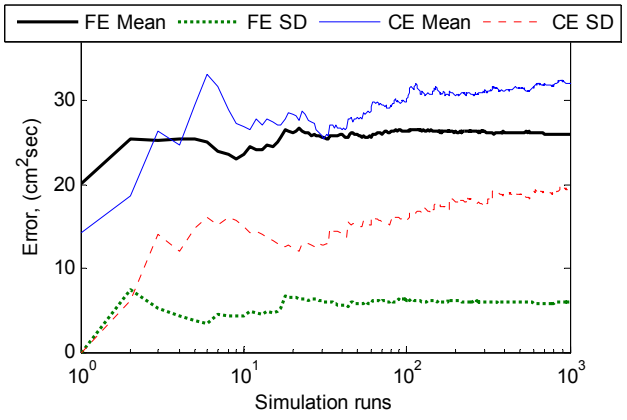

Fig. 6. Convergence rate of FE and CE.

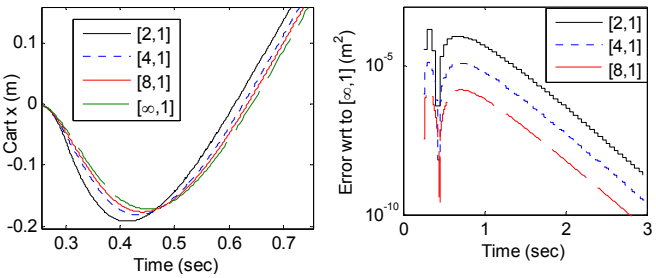

(a) Unit step response (b) Tracking error

Fig. 7. In absence of process and measurement noise.

Authorized licensed use limited to: IEEE Editors in Chief. Downloaded on February 5, 2010 at 14:16 from IEEE Xplore. Restrictions apply.

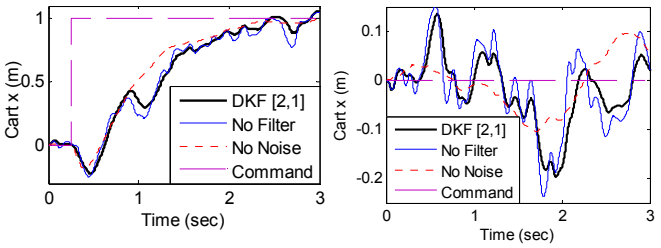

(a) Effects of DKF state estimates with [2, 1] configuration

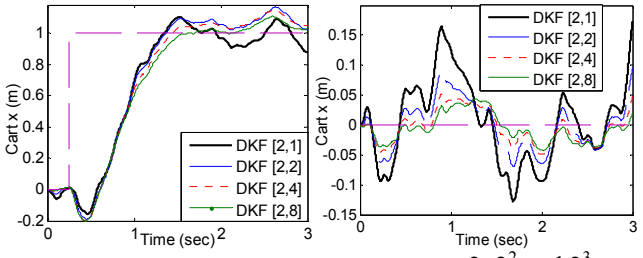

(b) Effects of redundancy [2, r], where r=1, 2, 2^2 and 2^3

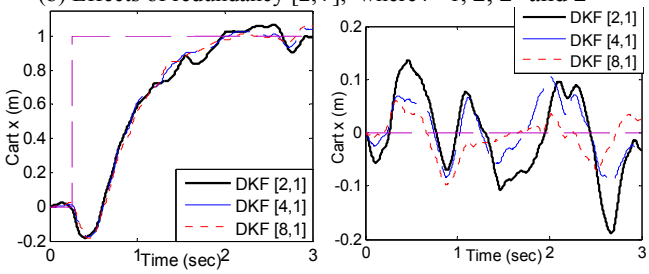

(c) Effects of sampling rate [s, 1] where s=2, 2^2 and 2^3

Fig. 8. Effects of configurations on cart displacement. (Left: unit step response. Right: steady-state response.)

Table 3: Effects of DKF on CE/ FE (Mean, SD) in [2,1] network.

Response	**Unit step** (cm^{2}sec)		**Steady- state** (cm^{2}sec)	
500 runs	CE	FE	CE	FE
No noise	7301, 499.3		43.30, 31.22	
No filter	7549, 973.2	666.2, 116.0	345.1, 175.	660.3,116.4
DKF	7475, 1091	323.1, 79.04	308.9, 182.	254.3, 58.10

Table 4: Effects of configuration on CE/FE (Mean, SD) with DKF.

Response	**Unit step** (cm^{2}sec)		**Steady- state** (cm^{2}sec)	
500 runs	CE	FE	CE	FE
[2,2]	710.3, 33.57	7.276, 1.141	34.53, 22.76	70.7, 10.59
[4,2]	721.1, 27.15	7.049, 0.781	18.84, 11.17	70.42, 7.64
[8,2]	726.8, 23.19	7.008, 0.552	11.18, 6.69	70.09, 5.32
[2,4]	710.8, 21.63	2.400, 0.349	12.00, 7.91	22.29, 3.13
[2,8]	710.4, 17.97	0.841, 0.113	6.23, 4.17	6.66, 0.90

The observations from the results are briefly summarized:

- Fig. 7 shows that in a noise-free environment, the tracking error is reduced by 2 orders when the number of sensor groups is doubled (or increasing from [2^1,1] to [2^2,1], and to [2^3,1]).
- Table 3 suggests that in an environment corrupted by Gaussian white noise, the filter lowers the CE and FE for both the unit step and steady-state response. In fact, the FE is halved when the DKF was used.
- As Table 4 suggests, for the steady-state case, the CE decreases with increasing sensor usage. While increasing the number of sensor groups from 2 to 8 (s) reduces the CE by almost 60%, performing the identical change to the sensors in each group (r) is more effective and results in a reduction of almost 80%. However, the CE for the unit step responses are unchanged with increasing redundancy and in fact higher at networks with higher s.
- The trend in the FE is similar to that of the CE. For both the unit step and steady-state cases, increasing the redundancy of the sensor network is more effective than increasing the network sampling rate in reducing the FE. Increasing the network redundancy from 2 to 8, reduces the FE reduced by 88% and 91% in the unit step and steady state case respectively. However, increasing the network sampling rate by the same factor could only muster an improvement in FE that is less than 5%.
- As depicted in Fig. 9, increasing the number of sensors in redundancy reduces the error in all cases except for the CE in the unit step case. On the other hand, the FE and CE for the unit step case is unaffected by the number of sensors in sequential mode. Increasing the number of sequential sensors is most effective in reducing the CE of the steady-state case.

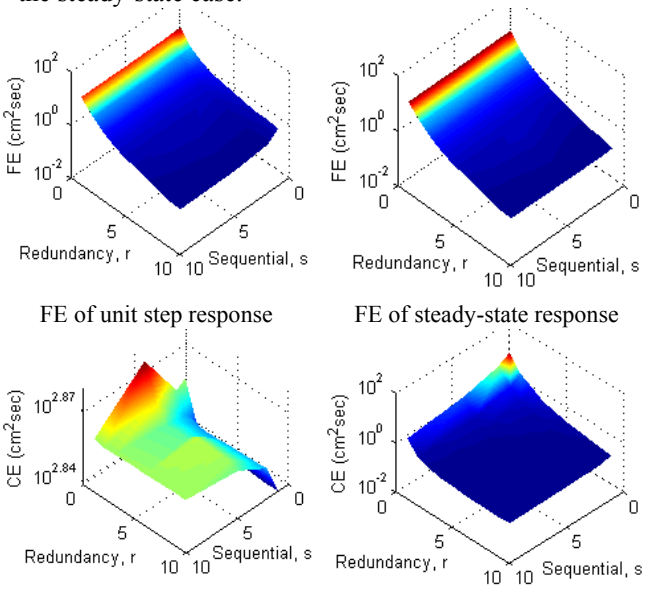

FE of unit step response | FE of steady-state response

CE of unit step response | CE of steady-state response

Fig. 9. Effects of r and s on CE and FE.

B. Throttling Controller Implementation

From the results of the previous section, it can be seen that configurations with higher number of sensors in redundancy improve steady state tracking of the system. This is largely due to the presence of the DKF and accurate knowledge of the controlling input into the inverted pendulum system which allows accurate prediction of the state during transient motion. Assuming the following minimum and maximum configurations are available: [2,1] and [2,5], a throttling sensor configuration controller that employs variable configurations using feedback from the DKF state estimate and desired command (16a) is described as follows,

$$r((k+1)T) = \begin{cases} 1 & \text{if } V(kT) \geq q \\ 5 & \text{otherwise} \end{cases} \qquad (19)$$

Authorized licensed use limited to: IEEE Editors in Chief. Downloaded on February 5, 2010 at 14:16 from IEEE Xplore. Restrictions apply.

where $V(kT) = |c(kT) - \hat{x}(kT)| / |c(kT) - \hat{x}(0)|$ and q is the threshold transition between the network configurations. This threshold determines the specific crossover point where the network switches between the maximum and minimum configurations. As performance of the overall organized sensor network is sensitive to the value of q, and reusing the CE and FE as a means to critique performance, 500 simulations of a delayed step input of the system with the throttling controller utilizing different values of q are compiled in Table 5. The case where q=0.1 is omitted because at steady state the natural variation of $\hat{x}(kT)$ caused by the noise in the system will inadvertently trigger the transient mode of the network. From the table, while employing the maximum configuration at all times, q=1, results in the lowest FE, it did not produce the lowest CE. Decreasing the value of q from 1 ([2,5]) towards 0 ([2,1]) results in increasing FE and decreasing sensor network utilization. The corresponding trend in CE is however nonlinear and a minimum occurs between the two extreme values of q. The throttling networks that resulted in the lowest CE are: q=0.3, 0.4, 0.5 and 0.6. The best performing throttling network occurs at q=0.5; and it outperformed [2,5] in CE and maintained an average sensor utilization of 88.3% when compared to [2,5].

Table 5: Effects of q on CE/FE (Mean, SD) in throttling network.

500 runs	q	CE (cm^2sec)	FE (cm^2sec)	Utilization (%)
[2,1]	0	777.5, 103.2	48.55, 9.618	20.0
Throttling	0.2	719.4, 54.82	18.69, 4.468	82.4, 3.55
	0.3	718.9, 54.67	17.57, 3.940	85.3, 2.19
	0.4	718.8, 54.59	16.87, 3.603	87.1, 1.67
	0.5	718.6, 54.58	16.29, 3.320	88.3, 1.41
	0.6	718.7, 54.87	15.80, 3.098	89.7, 1.23
	0.7	719.2, 55.03	15.33, 2.893	90.8, 1.08
	0.8	720.0, 55.13	14.89, 2.689	91.8, 1.01
	0.9	721.4, 54.88	14.46, 2.488	92.8, 0.97
[2,5]	1	730.8, 53.22	11.79, 1.360	100

The resulting response of the cart under a delayed unit step response using the throttling sensor controller (q=0.5) is shown in Fig. 10. The corresponding responses of the cart using the static configurations [2,1] and [2,5] are added for comparison. It can be seen that the throttling controller has the characteristics of both extreme configurations: The transient performance of cart under throttling controller is similar to that of [2,1] and the steady state performance is similar to that of [2,5].

IV. Conclusions

Using the inverted pendulum as a system platform, the feasibility of an organized sensor network to improve command tracking under feedback control was investigated. In simulations, it was found that while the system controlled by a DKF state feedback benefitted from additional sensors in the steady state case, the effect on the transient response of the system due to a unit step was statistically undetectable. Using this result, a throttling sensor network that uses least sensors in transient response and full complement of sensors at steady state was simulated. It was found that the transition between configurations affects the performance of the system and the system under throttling sensor network out performed the same system with static network while maintaining lower sensor utilization.

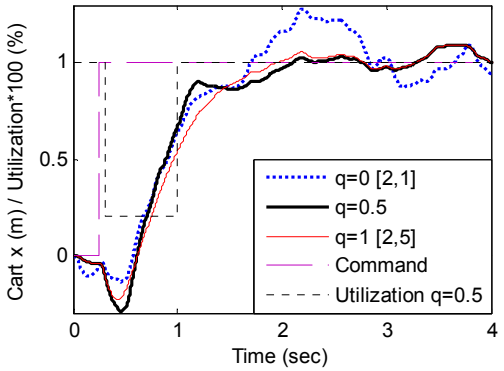

Fig. 10. Cart response and utilization under throttling network.

Acknowledgment

The project is jointly funded by the Georgia Agricultural Technology Research Program and the U. S. Poultry and Eggs Association.

References

[1] I. F. Akyildiz, W. Su, Y. Sankarasubramaniam, and E. Cayirci, "A Survey on Sensor Networks," *IEEE Communications Magazine*, vol. 40, pp. 102-114, Aug 2002.

[2] R. C. Luo, C-C. Yih, and K. L. Su, "Multisensor Fusion and Integration: Approaches, Applications, and Future Research Directions," *IEEE Sensors Journal*, vol. 2, no. 2, pp. 107-119, 2002.

[3] C.-Y. Chong, and S. P. Kumar, "Sensor Networks: Evolution, Opportunities, and Challenges," *Proceedings of IEEE*, vol. 91, no. 8, pp. 1247-1256, 2003.

[4] T. Arampatzis, J. Lygeros, and S. Manesis, "A Survey of Applications of Wireless Sensors and Wireless Sensor Networks," *Proceedings of IEEE Mediterranean Conference on Control and Automation*, pp. 719-724, Jun 2005.

[5] I. Infantino, A. Chella, H. Dzindo, and I. Macaluso, "Visual Control of a Robotic Hand," *Proceedings of the IEEE/RSJ International Conference on Intelligent Robots and Systems*, pp. 1266-1271, Las Vegas, Oct 2003.

[6] D. Willner, C. B. Chang, and K. P. Dunn, "Kalman Filter Algorithms for a Multi-Sensor System," *Proceedings of IEEE Conference on Decision and Control*, vol. 15, pp. 570-574, Nov 1976.

[7] W. Saidani, Y. Morsly and M. S. Djouadi, "Sequential Versus Parallel Architecture for Multiple Sensors Multiple Target Tracking," *Conference on Human System Interactions*, pp. 903-908, May 2008.

[8] S. Chroust, M. Vincze, R. Traxl, and P. Krautgartner, "Evaluation of Processing Architecture and Control Law on the Performance of Vision-Based Control Systems," *International Workshop on Advanced Motion Control*, 2000.

[9] E. M. Saad, M. H. Awadalla, M. A. Saleh, H. Keshk, and R. R. Darwish, "Adaptive and Energy Efficient Clustering Architecture for Dynamic Sensor Networks," *2nd International Workshop on Soft Computing Applications*, pp. 221-225, Aug 2007.

[10] K. Hirata, Y. Kimura, and K. Sugimoto, "Visual Feedback Control of Cart-Pendulum Systems with Webcam," *Proceedings of IEEE International Conference on Mechatronics*, pp. 1-6, May 2007.

[11] K. Hirata, and T. Mizuno, "Robust Visual Feedback Control of Inverted Pendulum System against Camera Misalignment," *10th IEEE International Workshop on Advanced Motion Control*, pp. 153-168, Mar 2008.

[12] A. Gelb, "Applied Optimal Estimation," MIT Press, 1974.

[13] Banner Engineering, "Vision Presence PLUS® Series," Banner Engineering Sensor Products Brochure, pp. 309-319.

Authorized licensed use limited to: IEEE Editors in Chief. Downloaded on February 5, 2010 at 14:16 from IEEE Xplore. Restrictions apply.